OPTIMAL LATERAL MANEUVERING FOR MICROBURST ENCOUNTERS DURING FINAL APPROACH

H.G. Visser

Delft University of Technology
Faculty of Aerospace Engineering
P.O. Box 5058, 2600 GB Delft
The Netherlands

Abstract

This paper is concerned with the control and optimization of lateral escape trajectories in a microburst wind field for an aircraft on final approach. The performance index being minimized is the peak value of altitude drop. An extensive numerical effort has been undertaken to investigate the characteristics of open-loop extremal solutions for different locations of the microburst. The results bear out that if lateral maneuvering is applied to turn the aircraft away from the microburst center, a significant improvement in the escape capability of the aircraft can be achieved in comparison to a straight flight. In contrast to non-turning escape maneuvers, optimal energy management often calls for an initial climb, rather than a descent, in a lateral escape maneuver. Finally, a feedback guidance scheme is proposed that closely approximates the open-loop trajectories.

I. Introduction

Weather phenomena that cause windshear, in particular the so-called "microburst", present a significant safety hazard during the take-off and landing of an aircraft. Such a microburst is a strong downdraft that strikes the ground, producing winds that diverge radially from the impact point (see Fig. 1). An airplane which penetrates the center of a microburst in straight flight will initially experience an increasing headwind and consequent upward force. As the aircraft proceeds along the glide slope, the downdraft increases and the headwind shifts into a tailwind causing the aircraft to loose speed and altitude (see Fig. 2).

Reactive windshear warning systems, which are gradually becoming standard fit aboard modern jet airliners, are capable of detecting such hazardous situations. When during final approach an aircraft is flying along the glide slope and such an inadvertent windshear situation is detected in a sufficiently early stage, the pilot may abort the landing and initiate an escape maneuver.

Research efforts which aim at establishing the optimal control strategy for such escape procedures have been conducted for some time now. However, most of these studies have focussed on controlling and optimizing flight trajectories in a vertical plane. Of particular interest in this context is the work of Miele et.al.. In addition to considering control strategies to improve the take-off and penetration landing performance during microburst encounter [2,3], Miele also specifically deals with the abort landing [4]. Reference [4] considers optimal (open-loop) trajectories through windshears and downdraft that minimize the peak value of the altitude drop, as well as closed-loop guidance strategies that closely approximate these open-loop optimal trajectories.

In Refs. 5 and 6, Zhao and Bryson propose an alternative formulation for the optimization of flight paths through microbursts, using a different performance measure. More specifically, paths are determined through windshears and downdrafts that maximize the final value of specific energy, while taking into account a minimum altitude constraint. It turns out that for strong-to-severe microbursts, the computed optimal paths are not essentially different from those found by Miele. In both cases the optimal strategy is (i) to initially descend to the minimum altitude, (ii) to remain in the vicinity of that minimum altitude, and (iii) to ascend once the aircraft has passed through the shear region.

Other dynamic optimization and flight guidance studies of considerable interest include those performed by Psiaki and Stengel, and by Hinton. The extensive parametric investigations of Psiaki and Stengel [7,8] have been particularly aimed at achieving a broad understanding of the factors that most strongly affect a microburst recovery, including variations in the microburst characteristics. Hinton [9] has examined a set of candidate strategies for recovery from microburst encounter, using both batch and piloted simulation. His findings indicate that in piloted operations, the performance of advanced optimal guidance laws (such as those developed by Miele et. al.) is not significantly better than the performance of simple strategies, such as the constant pitch technique. On the other hand, improving the alert time by just a few seconds was shown to lead to a significant performance increase.

The above optimization studies clearly indicate that early detection and warning of dangerous windshear significantly increases the survivability during final approach. For this reason substantial research efforts are currently being undertaken to develop so-called forward looking windshear detection systems which allow to look ahead of the aircraft [9,10]. In addition to improving the alert time, the availability of the information on the location of a microburst also offers the possibility of applying escape procedures involving lateral maneuvering. By turning the aircraft away from the microburst center, rather than flying straight through (see Fig. 3) the hazards caused by the penetration of a microburst can be reduced. These potential improvements were recently confirmed by a simulation study [11], in which flights with and without lateral maneuvering were compared. In this simulation study, the longitudinal strategy as recommended by the FAA Windshear training aid [12] was used, while lateral maneuvering was performed by commanding a constant bank angle of specified magnitude. Encouraged by these findings, the aim of the present study is to extend the work of Miele et. al. by computing optimal abort landing trajectories that feature lateral maneuvering. The characteristics of these trajectories are analyzed for the purpose of developing near-optimal escape guidance strategies.

In comparison to escape procedures which are restricted to flight in a vertical plane, the present formulation introduces an additional control variable, namely, bank angle. Although banking generally reduces the performance of an aircraft due to the required additional lift, banking may, however, also lead to a "positional advantage" within the microburst flow field. In addition to establishing an optimal escape strategy, it will also be of considerable interest to investigate to what extent lateral and longitudinal dynamics are actually coupled for such escape maneuvers.

Copyright © 1992 by ICAS and AIAA. All rights reserved.

II. Problem Formulation

Equations of Motion

Using a relative wind-axes reference-frame, the equations of motion, describing the aircraft dynamics (represented by a point-mass model) in the three-dimensional space can be written as:

$$\dot{x} = V\cos\gamma\cos\psi + W_x \tag{1}$$

$$\dot{y} = V\cos\gamma\sin\psi + W_y \tag{2}$$

$$\dot{h} = V\sin\gamma + W_h \tag{3}$$

$$\dot{E} = \frac{(T - D)V}{W} + \dot{W}_h - \frac{V}{g}\left[\dot{W}_x\cos\gamma\cos\psi + \dot{W}_y\cos\gamma\sin\psi + \dot{W}_h\sin\gamma\right] \tag{4}$$

$$\dot{\gamma} = \frac{g}{V}\left[\frac{L\cos\mu}{W} - \cos\gamma\right] + \frac{1}{V}\left[\dot{W}_x\sin\gamma\cos\psi + \dot{W}_y\sin\gamma\sin\psi - \dot{W}_h\cos\gamma\right] \tag{5}$$

$$\dot{\psi} = \frac{g}{V\cos\gamma}\frac{L\sin\mu}{W} + \frac{1}{V\cos\gamma}\left[\dot{W}_x\sin\psi - \dot{W}_y\cos\psi\right] \tag{6}$$

$$\dot{\beta} = \frac{1}{\tau}\left[\beta_t - \beta\right] \quad , \tag{7}$$

where x,y and h are the position coordinates, E is the specific energy, γ is the flight path angle, ψ the heading angle and β the throttle response. The wind velocity vector has three components, viz., W_x, W_y and W_h. The above equations embody the following assumptions: (i) a flat non-rotating earth, (ii) thrust T is aligned with the airspeed vector, (iii) the wind flow field is steady, (iv) the aircraft weight is constant. The throttle response is modeled as a first-order lag with a time constant τ. Note that since specific energy E is used here as a state variable, the airspeed V should be merely regarded as a function of energy E and altitude h, to be obtained from the relation:

$$E = h + \frac{V^2}{2g} \tag{8}$$

In the mathematical model the controls are:

(i) The throttle setting β_t constrained by:

$$0 \le \beta_t \le 1 \tag{9}$$

(ii) The bank angle μ which is limited by:

$$|\mu| \le \mu_{max} \tag{10}$$

(iii) The angle-of-attack α which is forced to remain within the range:

$$0 \le \alpha \le \alpha_{max} \tag{11}$$

The aerodynamic forces (lift L and drag D) are functions of airspeed V, altitude h and the angle-of-attack α:

$$L = C_L(\alpha)\ 0.5\ \rho(h)\ V^2 S \tag{12}$$

$$D = C_D(\alpha)\ 0.5\ \rho(h)\ V^2 S \tag{13}$$

Since the trajectories under investigation involve relatively modest variations in altitude, the maximum thrust is assumed to be a function of airspeed only, i.e.:

$$T = \beta\ T_{max}(V) \tag{14}$$

In this study a Boeing 727 point-mass model has been used, that was originally developed by Miele et. al. [2]. The characteristics of this aircraft model are summarized in Appendix A.

The Microburst Wind Model

The microburst model used herein is an axisymmetric three-dimensional extension of the two-dimensional model presented in Ref. 1. It actually features separate models for the radial flow (which may lead to horizontal shear) and the downdraft. Due to the axisymmetric character of the microburst model, it is convenient to use polar coordinates to describe the flow field in a horizontal plane (see Fig. 4). Using polar coordinates, the horizontal wind components W_x and W_y can be readily related to the radial wind velocity W_r:

$$W_x = \cos\psi_w\ W_r(r)\ ;\ W_y = \sin\psi_w\ W_r(r)\ , \tag{15}$$

where ψ_w is the direction of the radial wind velocity vector and r is the radial distance from the microburst center (axis of symmetry) located at the point (x_c, y_c), i.e.:

$$r = \{(x - x_c)^2 + (y - y_c)^2\}^{1/2} \tag{16}$$

Also note that in the present study the origin of the coordinate frame is located at the runway threshold. Unlike the radial flow model, the downdraft model features an additional dependence on the altitude, i.e.:

$$W_h = W_h(r, \psi_w, h) \tag{17}$$

In view of assumption (iii) in the previous Section, the total derivatives of these wind velocity components satisfy the relations:

$$\dot{W}_x = \frac{\partial W_x}{\partial x}\dot{x} + \frac{\partial W_x}{\partial y}\dot{y}\ ;\ \dot{W}_y = \frac{\partial W_y}{\partial x}\dot{x} + \frac{\partial W_y}{\partial y}\dot{y} \tag{18}$$

$$\dot{W}_h = \frac{\partial W_h}{\partial x}\dot{x} + \frac{\partial W_h}{\partial y}\dot{y} + \frac{\partial W_h}{\partial h}\dot{h} \tag{19}$$

An important characteristic parameter used in the evaluation of windshear performance is the so-called F-factor. Here we define this windshear hazard factor as:

$$F = \frac{(T - D)}{W} - \dot{E}/V \tag{20}$$

Defining the F-factor in this particular fashion permits its use in the analysis of both two-dimensional and three-dimensional windshear encounters. A Comparison of Eqs.(4) and (20) reveals that the F-factor can be readily interpreted as the loss or gain in available excess thrust-to-weight ratio due to the combined effect of downdraft and horizontal windshear. The F-factor therefore represents a direct measure of the degradation of an aircraft's climb gradient capability at constant speed caused by the presence of windshear/downdraft. Note that positive values of the F-factor indicate a performance decreasing situation. Further details concerning the microburst model and the F-factor can be found in Appendix B. The wind profiles corresponding to the model given in appendix B are shown in Fig. 5.

Optimization Criterion

Similar to Ref.4, the objective in this study is to minimize the peak value of the altitude drop, or, in other words, to maximize the minimum altitude reached by an aircraft (see Fig. 6):

$$I = \max_t\ (h_{ref} - h) \tag{21}$$

Following the approach of Ref.4, the minimax criterion in Eq.(21) is approximated by a Bolza performance index:

$$J = \int_0^{t_f} (h_{ref} - h)^n\ dt \quad , \tag{22}$$

where n is a large positive, even exponent. Note that for best possible computational results, the reference altitude h_{ref} should be chosen as small as possible, but such that the right-hand side of Eq.(21) remains positive at all times. The numerical values of the constants in Eq.(22) that have been used here are: n = 6 and h_{ref} = 400 m.

Boundary Conditions

The following initial conditions (at which the escape procedure is commenced) have been assumed in this study:

$$x(0) = x_0 = -2500 \text{ m}, \quad y(0) = y_0 = 0 \text{ m},$$
$$h(0) = h_0 = 131 \text{ m}, \quad E(0) = E_0 = 384.326 \text{ m},$$
$$\gamma(0) = \gamma_0 = -3^\circ, \quad \psi(0) = \psi_0 = 0^\circ,$$
$$\beta(0) = \beta_0 = 0.333 \qquad (23)$$

These values correspond to a situation in which an aircraft would fly during a stabilized approach (V = 70.5 m/s) without winds or windshear. It needs to be realized that in the presence of winds, the required values for γ_0 and β_0 will be somewhat different. However, since different locations of the microburst will be considered in the numerical examples, the above stated values will be assumed to apply in all situations, merely to achieve some degree of consistency. The final time t_f has been set to 50 seconds, which is sufficiently long to allow a transition of the shear region. No terminal boundary conditions have been imposed. Such conditions would mainly affect the extremal solution in the after-shear region. Our primary interest is in the control behavior during the passage of the shear region.

Optimal Control Problem

To summarize, the optimal control problem to be solved is to determine the optimal controls β_L^*, μ^* and α^* such that starting from the initial conditions of Eq.(23), the performance index of Eq.(22) is minimized for a given final time t_f.

Application of the first-order necessary conditions of Optimal Control theory [13] to the above stated problem results in a Two-Point-Boundary-Value-Problem (TPBVP), which is of considerable mathematical complexity. In the present study the extremals (solutions to the TPBVP) have been obtained iteratively using a highly accurate multiple-shooting algorithm [14]. At this point it is important to note, however, that such extremal solutions are merely candidates for local optimality. As a matter of fact, we have been able to find up to three extremals for a given set of boundary conditions in most cases. It is imperative to verify local optimality of these candidate extremals, by checking for the second-order necessary conditions (Jacobi-test). Such a test, together with the Legendre-Clebsch condition can provide assurance concerning the local optimality of candidate extremals. We emphasize, however, that, as yet, we have only concerned ourselves with computing candidate extremals.

III. Extremal Solutions

In order to investigate the characteristic features of the optimal escape trajectories, the principal parameters that have been varied in this study are the position coordinates (x_c, y_c) of the microburst center. The reference situation that has been selected concerns a microburst of which the center is located at (-1500m,0m). This implies that for the given initial conditions, an aircraft in straight flight will fly exactly along the x-axis of the reference frame (see Fig.4), passing right through the microburst center. Relative to this "symmetric" reference situation both the distance of the microburst center to the runway threshold (x_c coordinate position) and the lateral offset distance y_c have been varied within the range [-500m,+500m]. It is noted that extending this range is of limited value in the sense that such an extension will result in a situation which is either not survivable or does not pose a real safety hazard.

Reference Solution

In the Figs. 7 the results pertaining to the reference situation have been summarized. Due to the symmetry in the geometry of this microburst-encounter, it is not really surprising that the first converged extremal that was obtained simply was the optimal trajectory established earlier in the two-dimensional analysis [1], i.e., a straight flight along the x-axis. Initial efforts to compute lateral escape trajectories were unsuccessful in the sense that the TPBVP solutions failed to converge. It soon turned out that the only way in which lateral escape trajectories could be generated at all, was by specifying a fairly low value for the maximum bank angle μ_{max}. Indeed, for most of the considered encounters the maximum bank angle that can be specified is typically in the order of 15°. To demonstrate the impact of the maximum bank angle on the solution behavior, three different values for the maximum bank angle have been considered in Figs. 7, namely 5°, 10° and 15°. Moreover, due to symmetry considerations it is clear that lateral escape maneuvers can be performed by making either a left or a right turn. Consequently, it can be concluded that for any given (non-zero) value of the maximum bank angle, three different extremals can be found (left turn, right turn, straight flight).

Figure 7a shows the tracks for the escape maneuvers. It is noted that for the considered reference situation, the location of the microburst center is such that the initial conditions for the trajectory are near the maximum radial outflow velocity contour.

Figures 7b and 7c show the time-histories for the two control variables, angle-of-attack and bank angle. It is evident that all escape maneuvers are performed at full throttle and for this reason no plots for this third control variable have been included in this paper. The most striking feature in the observed angle-of-attack behavior is that in all cases about the same minimum value is reached at about the same time. The higher the specified maximum bank angle, the higher the initial angle-of-attack, while the maximum angle-of-attack is also reached earlier. The relatively high initial angle-of-attack for a lateral maneuver involving significant banking, results in a situation in which an initial climb is performed rather than a descent, as can be observed in Figure 7d. This behavior demonstrated by the turning extremals is fairly transparent. By converting kinetic energy into potential energy, the speed is reduced which will improve the turn rate (see Eq.(6)). As a result a positional advantage can be obtained by directing the flight away from the microburst center. It is noted that there is a close correspondence between the angle-of-attack behavior and the F-factor behavior (Fig. 7e). For example, maximum angle-of-attack is generally reached at the end of shear region (region with high F-values). In [10] a microburst is classified as hazardous if the average F-factor exceeds .1 over any 1 km segment. Using this as a yardstick, it is readily clear from Fig. 7e that the microburst encounter considered here easily qualifies as hazardous.

With respect to bank angle behavior, it can be observed that nearly all turning takes place in the initial phase. At some instance bank angle leaves its limit and decays to zero. The higher the value of the maximum bank-angle the earlier this decay sets in. Figure 7f shows the typical behavior of the corresponding heading angle time-history for one extremal. Generally speaking it can be observed that at the end of an escape maneuver, the projection of the aircraft's airspeed vector on a horizontal plane is more or less aligned with the radial wind velocity vector.

Figure 7g compares the airspeed behavior of escape trajectories with and without lateral maneuvering. Although in the initial phase the airspeed is lower for the lateral escape maneuver, specific energy is actually well-managed in this maneuver. As a matter of fact, at termination the specific energy is significantly higher for the lateral maneuver than for the non-turning maneuver.

The improvements in performance that can be obtained by executing a lateral escape maneuver are significant, as can be observed from Fig. 7d. The minimum altitude reached at any point along the trajectory has been plotted as a function of the specified maximum bank angle in Fig. 7h (exact solution). The results clearly indicate that even better results can be expected for higher values of the specified maximum bank angle. As already mentioned earlier, we have, unfortunately, not been able to obtain such solutions.

Effect of a Lateral Microburst Displacement

A second numerical example of extremal behavior concerns a situation in which the center of the microburst is offset from the x-axis of the reference frame. In this particular example, the lateral microburst displacement y_c is set to 100m. The results are illustrated in Figs. 8.

The ground tracks shown in Fig. 8a do no longer exhibit a symmetry relative to the x-axis. In other words, there is now a need to distinguish between left and right turns. However, we still have the situation that there are generally three different extremals for a given value of the maximum bank angle (provided this value is sufficiently large).

First of all, there is an "unconstrained" extremal, which, like in the reference solution, passes right through the microburst center. In order to achieve this, some initial banking is required for this extremal, as shown in Fig. 8c. A second type of extremals concerns escape trajectories involving a turn to the right, or, in other words, a turn towards the microburst center. Finally, a third type of extremals that can be found concerns trajectories featuring a turn to the left, or, in other words, a turn away from the microburst center. For a given value of the maximum bank angle, the optimal angle-of-attack behavior is quite different for a left and a right turn, as can be observed from Fig. 8b, where results are shown for $\mu_{max} = 10^\circ$. A striking feature is that the angle-of-attack behavior of the escape maneuver to the left results in an initial "zoom-climb", as can be seen in Fig. 8d.

Not surprisingly, escape maneuvers to the left, in which aircraft are turned away from the microburst center, lead to a much better performance. In fact, Fig. 8d makes clear that turning to the right even leads to a lower minimum altitude than not turning at all. Figure 8e shows the minimum altitude reached at any point along the trajectory as a function of the specified maximum bank angle. Note that the curve shown in this figure is interrupted. The reason for this is that it proved to be impossible to compute escape trajectories that involve a turn to the right, but which pass the microburst center to the left. Note that the minimum altitude obtained for the unconstrained solution ($h_{min} = 42.3$m) is about 1.7m higher than for the lowest minimum altitude obtained for a constrained solution ($h_{min} = 40.6$m, for a right turn with $\mu_{max} = 10^\circ$).

In addition to comparing the minimum altitudes achieved in turning and non-turning escape trajectories, we have also looked at alternative ways to express the performance improvements. For example, the minimum altitude achieved in a lateral escape maneuver to the left with $\mu_{max} = 10^\circ$ is about 15m higher than the minimum altitude achieved in an escape maneuver with bank angle fixed at zero degrees. This corresponds to a reduction in the required advance warning time of about 2.4 seconds. This particular result has been obtained by delaying the initiation of the lateral escape maneuver while proceeding along the glide slope, such that the resulting minimum altitude is equal to the minimum altitude obtained for the non-turning trajectory. Alternatively, the lateral escape maneuver can be flown with an 8% increase in the windshear intensity and still achieve the same performance as the non-turning trajectory in this particular example.

Effect of Displacing a Microburst Forward/Backward

This particular example serves to demonstrate the effect of displacing the center of the microburst forward/backward relative to the runway threshold. In this example the lateral microburst displacement y_c is set to -150m, while all escape maneuvers are executed by making a right turn with $\mu_{max} = 10^\circ$. The results are illustrated in the Figs. 9.

Fig. 9a shows the ground tracks of the three considered extremals. Note that one extremal starts well within the peak radial outflow velocity contour ($x_c = -1750$m), whereas another starts well outside this contour ($x_c = -1250$m).

Figures 9b and 9c show the control solutions. It is readily observed that the closer the microburst center is located to the threshold, the higher the initial angle-of-attack. Indeed, if the maneuver is initiated well outside the maximum radial outflow velocity contour, the aircraft can initially climb without experiencing a significant downdraft. Since in the presently employed model the vertical wind speed depends linearly on the altitude, climbing is clearly not advisable within the downdraft region. This helps to explain the relatively large differences in altitude behavior that can be observed between the three extremals (Fig. 9d). Not surprisingly the differences in performance are also considerable.

Influence of Initial Airspeed

The final example is intended to further illustrate the energy management features of lateral escape maneuvers. In this example the same geometry of the microburst encounter is considered as in the reference situation, but here the initial condition on airspeed has been varied. The results pertaining to three different values of initial airspeed are presented in the Figs. 10. Figure 10a shows that the lowest initial angle-of-attack is found for the extremal with the highest initial airspeed. However, Fig. 10b reveals that the overall influence of initial airspeed is such that a higher lift will be developed in the initial phase of the escape maneuver, when it is initiated with a higher airspeed. In other words, any increase in initial kinetic energy will be largely converted to potential energy such as to improve the turn rate in the initial phase.

IV. Guidance Solutions

In this Section a closed-loop guidance scheme is derived which approximates the open-loop optimal trajectories, relying on local (measurable) wind information only. With respect to the angle-of-attack, several guidance laws have been developed for near-optimal escape maneuvering in a vertical plane [4], which could have been used as a starting-point for the present analysis. However, in view of the findings of Ref.[9], where advanced guidance laws were shown to offer little performance improvement in piloted simulation in comparison to a baseline constant pitch technique, it was decided to start out with the latter approach. Moreover, the altered angle-of-attack behavior due to lateral maneuvering that was observed in the optimal trajectory analysis, suggests that in order to account for such coupling effects, a significant modification of the advanced pitch strategies is probably called for anyway.

The simple constant pitch technique is used here in conjunction with a newly derived guidance law for the bank angle. From the behavior of the optimal trajectories (see, e.g., Figs. 7c and 7f) it was inferred that the guidance law for the bank angle should take the following simple form:

$$\mu = K\,(\psi_w - \psi)\,, \quad |\mu| \le \mu_{max}\,, \tag{24}$$

with the gain coefficient K selected as 0.25 and where it is understood that:

$$-180^\circ \le \psi_w \le 180^\circ, \quad -180^\circ \le \psi \le 180^\circ \tag{25}$$

The constant pitch guidance is based on a target pitch, where:

$$\theta_{ref} = 15^{\circ} \qquad (26)$$

The feedback control scheme in Fig. 11 shows the the implementation of the guidance laws.

A substantial simulation effort has been undertaken to validate the proposed guidance laws. Analysis of the simulated feedback trajectories reveals a characteristic control behavior very similar to that of open-loop extremals (assuming these correspond to turning in the "correct" direction). For a particular case, namely, the reference situation with $\mu_{max} = 15^{\circ}$, the Figs. 12a and 12b show a comparison of the control behavior. Figure 12c shows the corresponding altitude behavior. Although there is clearly room for improvement, overall the proposed feedback strategy leads to a satisfactory performance. Moreover, unlike for the optimal trajectory computation, in the feedback trajectory simulations there are no numerical complications that prohibit specifying values for the maximum bank angle larger than 15°. This is shown in Fig. 7h, where a comparison of the minimum altitude as a function of the specified maximum bank angle is made between feedback approximations and exact open-loop solutions (reference situation). It is clear that in this particular case even further performance improvements can be expected, by allowing bank angles in excess of 30°. Especially for higher values of the specified maximum bank angle, the simulated feedback results are remarkably close to the open-loop optimal results.

V. Conclusions

Optimal lateral escape trajectories in a microburst wind field were studied for an aircraft on final approach. The performance index being minimized was the peak value of altitude drop. A simple, yet realistic, microburst model was used and different microburst locations were assumed. Full thrust was applied in all cases, so that only angle-of-attack and bank angle remained as control variables in the point-mass model.

Unfortunately, we have not been able to generate lateral escape trajectories with a specified maximum bank angle larger than 15°. However, for a specified value of the maximum bank angle of that magnitude, typically three extremal solutions can be found, namely one trajectory passing the microburst center to the left, one trajectory passing the center to the right and one that passes right through the center. This behavior is found, regardless whether the microburst center is laterally displaced or not.

Provided the aircraft turns away from the microburst center, lateral maneuvering leads to a significant improvement in the escape capability of the aircraft, even when the maneuver is initiated within the peak radial outflow velocity contour. On the other hand, in case of a flight with a lateral microburst displacement, incorrect lateral maneuvering may result in a performance loss.

One of the most striking results established in this study relates to the energy management features of lateral maneuvering. In contrast to escape maneuvers that take place in a vertical plane only, lateral escape maneuvers often exhibit an initial climb. It is believed that this climb permits an energy-efficient speed reduction, which is then exploited to improve the turn rate. In other words, in an optimal lateral escape maneuver the best overall compromise between the conflicting requirements of a high turn rate (to take the aircraft away from the microburst center) and a low energy bleed-off rate (to maintain climb-gradient capability) is established .

A simple guidance scheme has been examined. Despite its simplicity, the guidance scheme produces a control behavior which closely resembles that of open-loop optimal solutions, in particular for higher values of the specified maximum bank angle.

It should be noted that the present investigations are essentially theoretical in nature and are primarily aimed at obtaining insight into the energy management features of optimal lateral escape maneuvers. It is clear that a substantial research effort is still required before it is meaningful to address operational aspects.

Appendix A: Boeing 727 Model

The model of a B-727 aircraft formulated by Miele [2,3,4], converted to SI units, is used here:

$W = 667233$ N , $S = 144.9$ m^2, $\tau = 3$ sec.

$$T_{max} = T_0 + T_1 V + T_2 V^2 \quad (N)$$

with : $T_0 = 198280$ N
$T_1 = -350.08$ N(m/s)$^{-1}$
$T_2 = 0.69063$ N(m/s)$^{-2}$

$$C_D = D_0 + D_1 \alpha + D_2 \alpha^2 \qquad (\alpha \text{ in radians})$$

with : $D_0 = 0.15751$
$D_1 = 0.0768$ rad^{-1}
$D_2 = 2.524$ rad^{-2}

$$C_L = L_0 + L_1 \alpha + L_2 (\alpha - \alpha_{ref})^2$$

with : $L_0 = 0.7076$
$L_1 = 5.97$ rad^{-1}
$L_2 = 0$ if $\alpha \le \alpha_{ref}$
$= -5.95$ rad^{-2} if $\alpha > \alpha_{ref}$

$$\alpha_{ref} = 0.2269 \text{ rad.}$$

The 1962 U.S. standard atmosphere [1] has been used throughout this study.

Appendix B: A simple analytic microburst model

In the present study a simple analytic approximation of the flow field characteristics of the microburst is employed. The induced radial and vertical velocities at any point in the three-dimensional space can be computed through the following relations:

$$W_r = f_r \left[\frac{-100}{\left(\frac{r + D/2}{200}\right)^2 + 10} + \frac{100}{\left(\frac{r - D/2}{200}\right)^2 + 10} \right] ;$$

$$W_h = f_h \left[\frac{-0.4\, h}{(r/400)^4 + 10} \right] \qquad (m/s) \qquad (b.1)$$

The parameters f_r, f_h characterize the intensity of the horizontal shear and downdraft respectively (the parameters f_r and f_h have the value 2 in the examples presented in this work). The parameter D specifies the radius of the peak horizontal outflow velocity contour (in this study D is taken as 2000 m).

Using polar horizontal position coordinates, the F-factor in Eq.(20) can be conveniently expressed as:

$$F = \frac{\cos\gamma}{g} \left(V\cos\gamma \left[\frac{\partial W_r}{\partial r} \cos^2(\psi - \psi_w) + (W_r/r) \sin^2(\psi - \psi_w) \right] + W_r \frac{\partial W_r}{\partial r} \cos(\psi - \psi_w) \right) + \frac{\sin\gamma}{g} \left(\frac{\partial W_h}{\partial r} \left[W_r + V\cos\gamma \cos(\psi - \psi_w) \right] + \frac{\partial W_h}{\partial h} \left[W_h + V\sin\gamma \right] \right) - \dot{W}_h / V \qquad (b.2)$$

It is noted that the F-factor does not merely depend on the spatial location within the flow field, but rather on all state variables. In Fig.B.1 the F-factor is plotted as a function of the radial distance r and the "wind incidence angle" $(\psi_w - \psi)$ for a given altitude, speed, and flight path angle.

References

1 Soesman, J.L, "Control of Aircraft Through Windshear During Final Approach", NLR Report TR 90117 L, 1990.

2 Miele, A., Wang, T. and Melvin, W.W., "Optimization and Acceleration Guidance of Flight Trajectories in a Windshear", Journal of Guidance, Control, and Dynamics, Vol.10, July-August 1987, pp. 368-377.

3 Miele, A., Wang, T. and Melvin, W.W., "Penetration Landing Guidance Trajectories in the Presence of Windshear", Journal of Guidance, Control, and Dynamics, Vol.12, Nov.-Dec. 1989, pp. 806-814.

4 Miele, A., Wang, T., Melvin, W.W. and Bowles, R.L., "Acceleration, Gamma and Theta Guidance for Abort Landing in a Windshear", Journal of Guidance, Control, and Dynamics, Vol.12, Nov.-Dec. 1989, pp. 815-821.

5 Zhao,Y. and Bryson, A.E., "Optimal Paths Through Downbursts", Journal of Guidance, Control, and Dynamics, Vol.13, Sept.-Oct. 1990, pp. 813-818.

6 Zhao,Y. and Bryson, A.E., "Control of an Aircraft in Downbursts", Journal of Guidance, Control,and Dynamics, Vol.13, Sept.-Oct. 1990, pp. 819-823.

7 Psiaki, M.L. and Stengel, R.F., "Optimal Flight Paths Through Microburst Wind Profiles", Journal of Aircraft, Vol.23, August 1986, pp. 629-635.

8 Psiaki, M.L. and Stengel, R.F., "Optimal Aircraft Performance During Microburst Encounter", Journal of Guidance, Control,and Dynamics, Vol.14, March-April 1991, pp. 440-446.

9 Hinton, D.A. "Forward-Look Wind-Shear Detection for Microburst Recovery", Journal of Aircraft, Vol.29, Jan.-Feb. 1992, pp. 63-66.

10 Bowles, R.L., Reducing Windshear Risk Through Airborne Systems Technology, Proceedings of the 17th ICAS, Stockholm, 1990, pp. 1603-1630.

11 Avila de Melo, D. and Hansman, R.J., "Analysis of Aircraft Performance During Lateral Maneuvering for Microburst Avoidance", Journal of Aircraft, Vol.28, Dec. 1991, pp. 837-842.

12 Federal Aviation Administration Windshear Training Aid, U.S. Dept. of Transportation, Associate Administration for Development and Logistics, Washington DC, 1987.

13 Bryson, A.E. and Ho, Y.-C., "Applied Optimal Control", Hemisphere Publishing Corporation, Washington, 1975.

14 Grimm, W., Berger, E. and Oberle, H.J., "Benutzeranleitung fur das Rechenprogram BNDSCO zur Losung Beschrankter Optimaler Steuerungsprobleme", DFVLR-Mitt. 85-05, 1984.

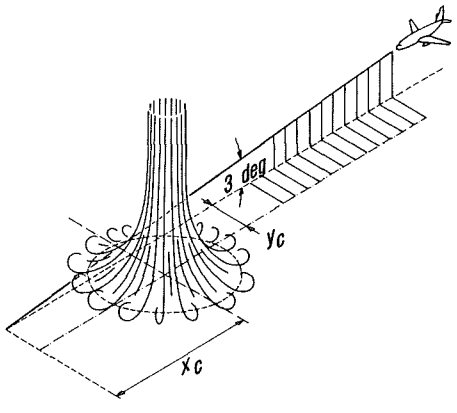

Fig. 1 Microburst encounter during final approach.

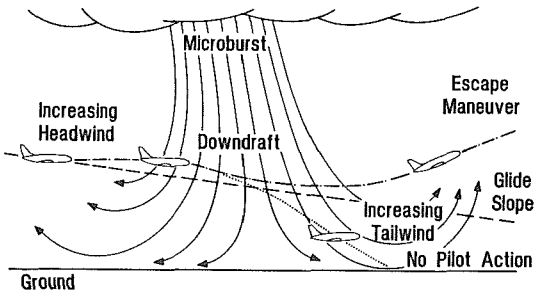

Fig. 2 Straight flight through a microburst.

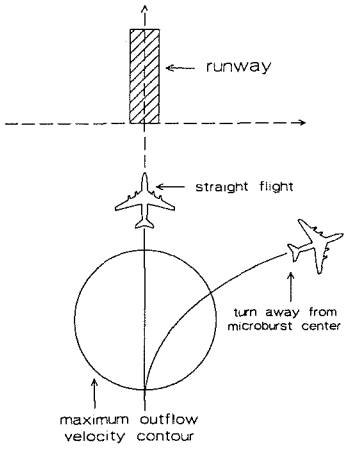

Fig. 3 Escape with and without lateral maneuvering.

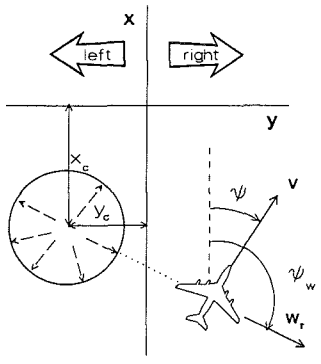

Fig. 4. Geometry of microburst encounter.

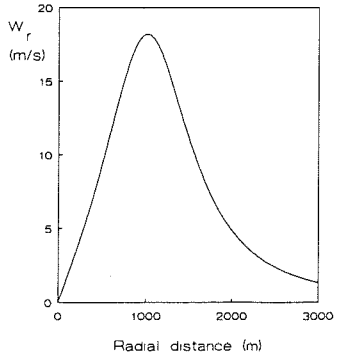

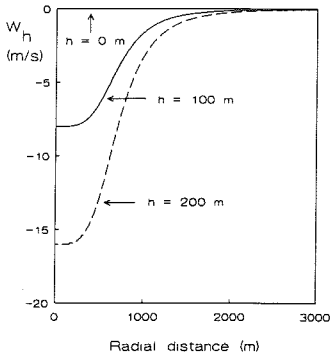

Fig. 5 Horizontal and vertical wind velocity profiles.

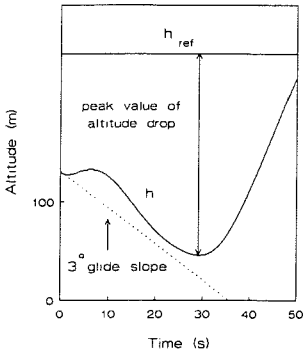

Fig. 6 Performance index.

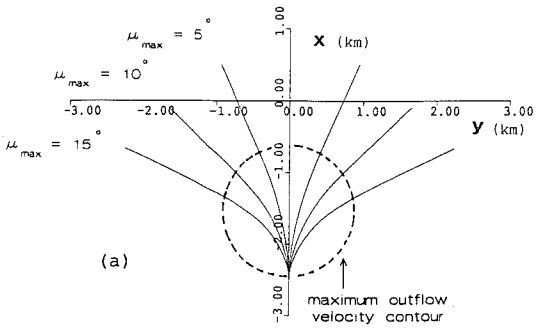

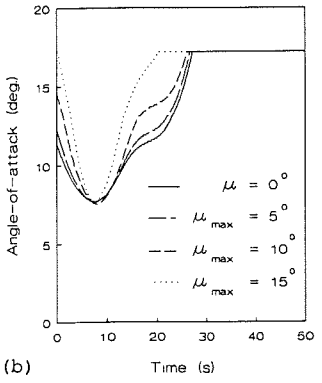

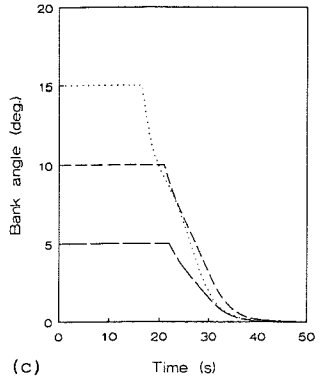

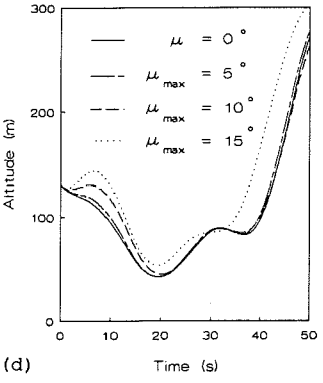

Fig. 7 Comparison of extremal solutions for various values of the maximum bank angle (reference solution). Distance of the microburst center to the runway threshold is 1500 m. No lateral displacement.

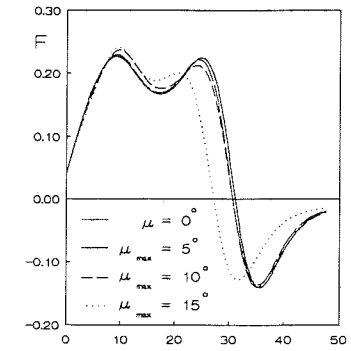

(e)

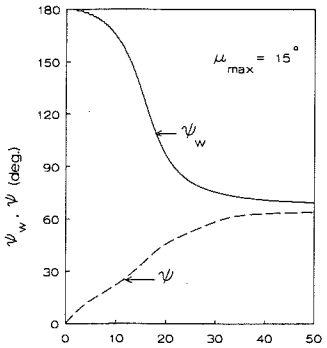

(f)

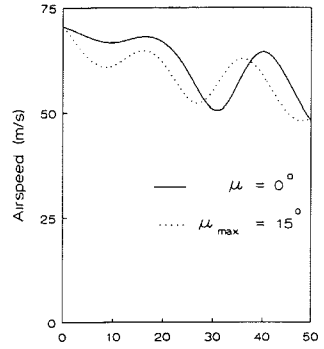

(g)

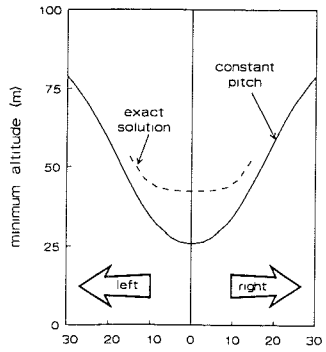

(h)

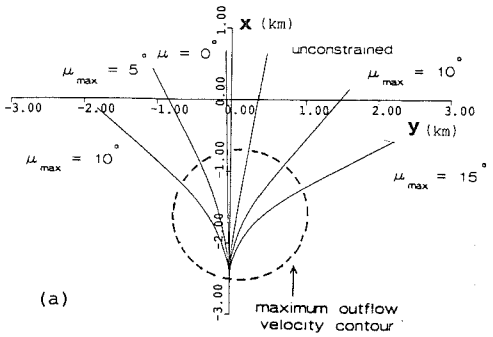

(a)

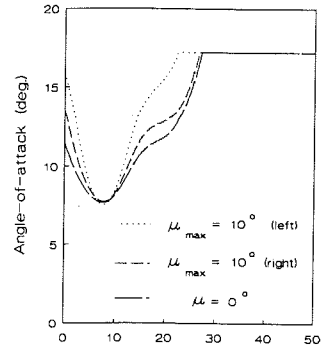

(b)

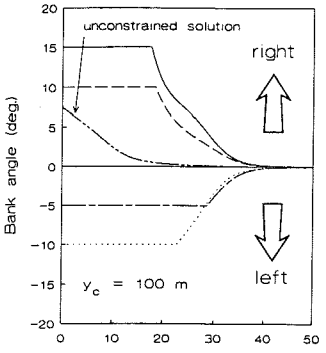

(c)

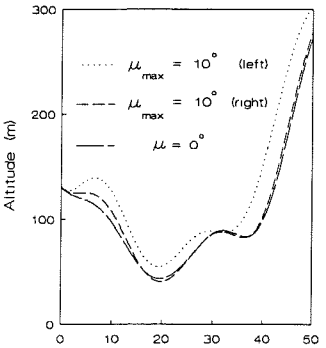

(d)

Fig. 7 Comparison of extremal solutions for various values of the maximum bank angle (reference solution). Distance of the microburst center to the runway threshold is 1500 m. No lateral displacement. (Continued).

Fig. 8 Comparison of extremal solutions for various values of the maximum bank angle. Distance of the microburst center to the runway threshold is 1500 m. The lateral displacement y_c is 100m.

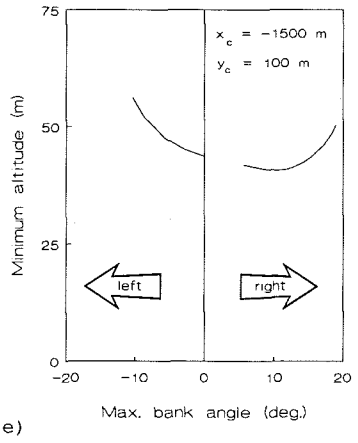

(e)

Fig. 8 Comparison of extremal solutions for various values of the maximum bank angle. Distance of the microburst center to the runway threshold is 1500 m. The lateral displacement y_c is 100m. (Continued).

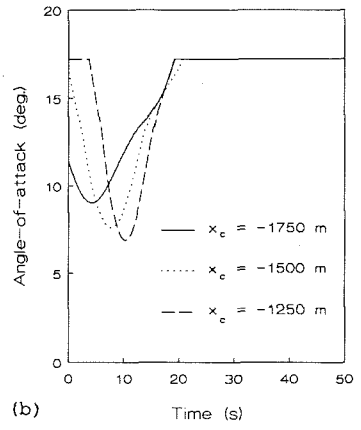

(b)

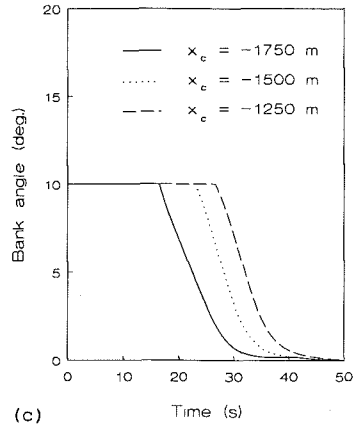

(c)

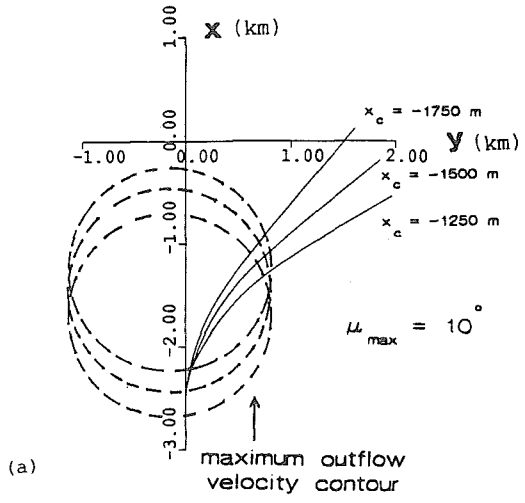

(a)

Fig. 9 Comparison of extremal solutions for various values of the distance of the microburst center to the runway threshold is 1500 m. The lateral displacement y_c is -150m. The maximum bank angle is 10 deg.

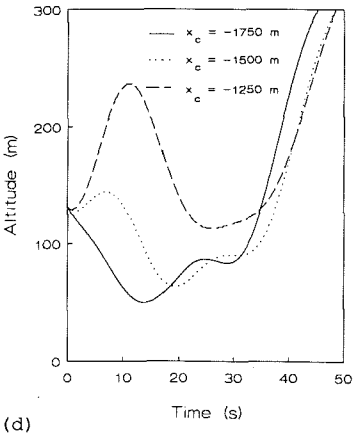

(d)

Fig. 9 Comparison of extremal solutions for various values of the distance of the microburst center to the runway threshold is 1500 m. The lateral displacement y_c is -150m. The maximum bank angle is 10 deg. (Continued).

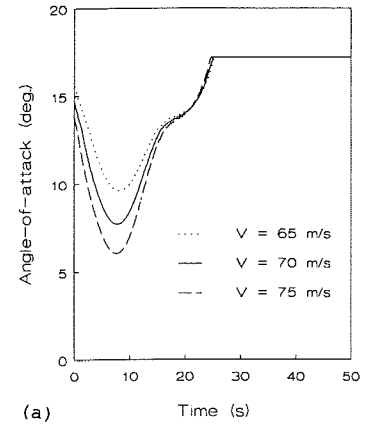

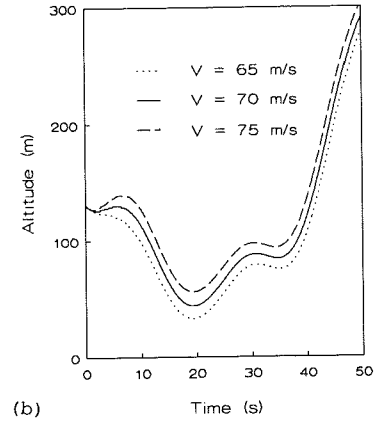

Fig. 10 Comparison of extremal solutions for various values of the initial airspeed. The distance of the microburst center to the runway threshold is 1500 m. There is no lateral displacement. The maximum bank angle is 10 deg.

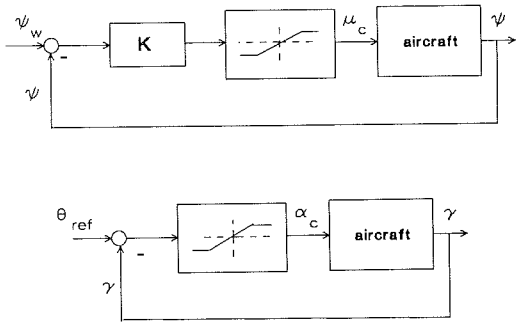

Fig. 11 Feedback guidance laws.

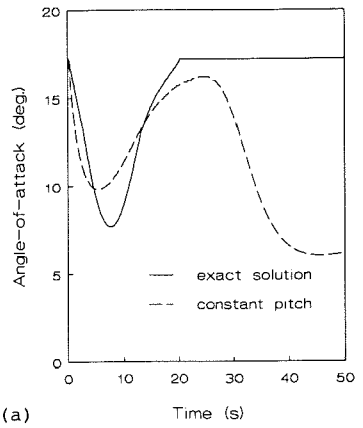

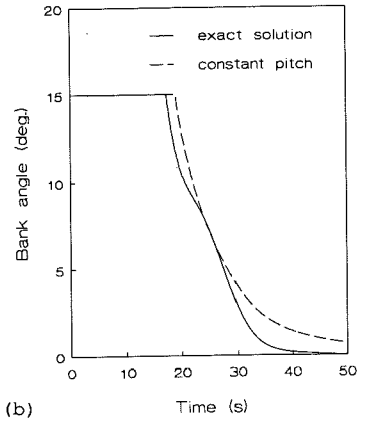

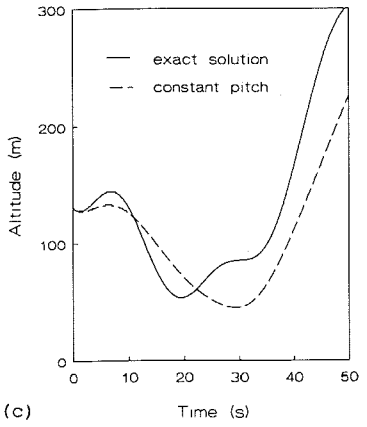

Fig. 12 Comparison between a simulated feedback solution and an exact open-loop optimal solution. The distance of the microburst center to the runway threshold is 1500 m. There is no lateral displacement. The maximum bank angle is 15 deg.

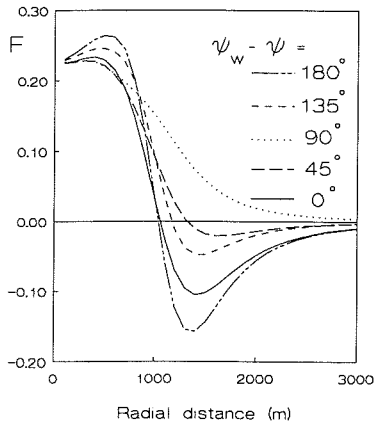

Fig. B.1 The F-factor as a function of the radial distance to the microburst center, for several values of the wind incidence angle $\psi_w - \psi$, where it is assumed that V = 70 m/s, h = 100 m and $\gamma = -3°$.